

# Targeted Ultrasound Nanobubbles Therapy for Prostate Cancer via Immuno-Sonodynamic Effect

Xin Huang, Yueying Chen, Fanglu Zhong, Bin Gui, Yugang Hu, Yuxin Guo, Qing Deng, Qing Zhou

Department of Ultrasound, Renmin Hospital of Wuhan University, Wuhan, 430060, People's Republic of China

Correspondence: Qing Zhou; Qing Deng, Department of Ultrasound, Renmin Hospital of Wuhan University, 238# Jiefang Road, Wuhan, 430060, People's Republic of China, Email [qingzhou@whu.edu.cn](mailto:qingzhou@whu.edu.cn); [wudadq@163.com](mailto:wudadq@163.com)

**Background:** Prostate cancer (PCa) poses a significant global health threaten. Immunotherapy has emerged as a novel strategy to augment the inhibition of tumor proliferation. However, the sole use of anti-PD-L1 Ab for PCa has not yielded improvements, mirroring outcomes observed in other tumor types.

**Methods:** This study employed the thin film hydration method to develop lipid nanobubbles (NBs) encapsulating chlorin e6 (Ce6) and anti-PD-L1 Ab (Ce6@aPD-L1 NBs). Our experimental approach included cellular assays and mouse immunization, providing a comprehensive evaluation of Ce6@aPD-L1 NBs' impact.

**Results:** The Ce6@aPD-L1 NBs effectively induced reactive oxygen species generation, leading to tumor cells death. In mice, they demonstrated a remarkable enhancement of immune responses compared to control groups. These immune responses encompassed immunogenic cell death induced by sonodynamic therapy and PD-1/PD-L1 blockade, activating dendritic cells maturation and effectively stimulating CD8+T cells.

**Conclusion:** Ce6@aPD-L1 NBs facilitate tumor-targeted delivery, activating anti-tumor effects through direct sonodynamic therapy action and immune system reactivation in the tumor microenvironment. Ce6@aPD-L1 NBs exhibit substantial potential for achieving synergistic anti-cancer effects in PCa.

**Keywords:** Ce6, nanobubbles, ultrasound, sonodynamic therapy, immunotherapy

## Introduction

Prostate cancer (PCa) stands as a hormonally driven malignancy and ranks as the second most frequently diagnosed cancer in men globally.<sup>1</sup> Androgen deprivation therapy emerges as a crucial treatment for patients with locally advanced and metastatic PCa, yet almost all patients eventually develop androgen-independent PCa.<sup>2</sup> Another therapeutic avenue is chemotherapy, with docetaxel (DTX) being the established first-line cytotoxic drug proven to extend overall survival.<sup>3,4</sup> However, the utilization of DTX-based chemotherapy may face limitations due to drug resistance and severe side effects, encompassing anaphylaxis, myelosuppression, gastrointestinal toxicity, and neurotoxicity.<sup>5</sup>

Since patients no longer amenable to surgical cure and exhibiting poor responsiveness to medical therapy, impeding tumor growth becomes pivotal in mitigating disease progression. Tumor immunosuppression, intricately linked with the tumor microenvironment (TME), expedites tumor growth.<sup>6</sup> Consequently, immunotherapy emerges as a novel treatment strategy to augment the inhibition of tumor proliferation. Immune checkpoints, including programmed cell death 1 (PDCD1/PD-1) and programmed cell death 1 ligand 1 (PDCD1LG1/PD-L1), play pivotal roles in mediating tumor immunosuppression.<sup>7</sup> Leveraging immune checkpoint blockade (ICB), anti-PD-L1 Ab are progressively employed to prevent tumor cells from evading the immune system, presenting a promising and viable strategy for tumor eradication.<sup>8</sup> However, PD-L1 expression is not exclusive to tumor cells but also found in normal tissues like vascular endothelial cells, hepatocytes, and mesenchymal stem cells.<sup>9</sup> Thus, conventional intravenous injections of free anti-PD-L1 Ab may lead to non-target interactions with normal tissues. Such non-targeted combinations not only result in low concentrations

in the tumor but also give rise to immune-related adverse effects, including endocrine diseases, skin toxicity, and gastrointestinal symptoms.<sup>10,11</sup>

For achieving high concentrations in the tumor while ensuring the safe use of anti-PD-L1 Ab, the development of a tumor-targeting anti-PD-L1 Ab delivery system is imperative. Microbubbles (MBs) have the capability to transport drugs or genes to tumor, and ultrasound (US)-targeted MB destruction (UTMD) enhances the therapeutic efficacy.<sup>12</sup> However, the size of MBs, typically ranging from 1–4  $\mu\text{m}$ , limits their penetration into tumor tissues. On the other hand, nanobubbles (NBs) with a size of 100–500 nm can passively accumulate in tumor tissues through the enhanced permeability and retention (EPR) effect. NBs loaded with anti-PD-L1 Ab can bind to tumor cells, facilitating targeted aggregation of NBs within the tumor. The cavitation effect generated by NBs under US irradiation further promotes the release of anti-PD-L1 Ab.<sup>13</sup>

While anti-PD-L1 Ab have been employed in clinical experiments for treating patients with PCa, the observed improvements have been lower in proportion and level compared to other tumor types.<sup>14</sup> Consequently, the objective of our research was to identify methods to enhance treatment effectiveness. Leveraging the characteristics of NBs and UTMD, we aimed to achieve sonodynamic therapy (SDT) through US irradiation. SDT has the potential to induce immunogenic cell death (ICD) of tumor cells, reinitiating an anti-tumor immune response. Additionally, SDT inflicts damage on tumor cells under US irradiation with sonosensitizers.<sup>15</sup> US irradiation enhances cell membrane permeability, thereby contributing to the efficient cellular uptake of drugs.<sup>16</sup>

Chlorine e6 (Ce6) a stable degradation product of chlorophyll-a (the main component of green plants), possesses a four-pyrrole ring structure that readily absorbs light. Recognized as a top-tier photosensitizer and sonosensitizer in nature, Ce6 offers the advantages of being non-toxic, exhibiting good specificity, and rapid metabolism.<sup>17</sup> Furthermore, Ce6 is a representative and promising sonosensitizer,<sup>18</sup> which has been used to treat solid tumors in the animal study.<sup>19</sup> The free form of Ce6, when intravenously injected into the body, fails to selectively concentrate in lesions. Therefore, nanotechnology modifications are essential to improve the tissue selectivity of free Ce6.<sup>20</sup> Previous researches have confirmed that Ce6 could be assembled well onto the surface of NBs, and effectively promoted the generation of reactive oxygen species (ROS) under US irradiation.<sup>21</sup>

The initial step in constructing targeted NBs is the effective conjugation of Ce6 and anti-PD-L1 Ab. Avidin-biotin serves as the preferred conjugation mode in research due to several advantages. Notably, the avidin-biotin affinity surpasses that of antigen-antibody interactions.<sup>22</sup> Furthermore, avidin's four binding sites facilitate increased loading of anti-PD-L1 Ab.<sup>23</sup> Additionally, considering that free Ce6 is insoluble in water but soluble in lipids, and since NBs share the same composition, this conjugation approach aligns well with the characteristics of the components. Following this rationale, we constructed tumor-targeted NBs encapsulating anti-PD-L1 Ab and Ce6 (Ce6@aPD-L1 NBs) to validate their anti-tumor effects through in vitro and in vivo experiments.

Upon reaching the tumor via passive and active targeting modalities, Ce6@aPD-L1 NBs effectively inhibit tumor growth. This inhibition is attributed not only to the direct action of SDT but also to the reactivation of the immune system, enhancing immune responses within the TME. The synergistic immunotherapy involves ICD induced by SDT, leading to the translocation of calreticulin (CRT) to the surfaces of tumor cells. This process activates dendritic cells (DCs) and stimulates CD8+T cells, thereby enhancing the release of various tumor immune factors. In summary, these promising Ce6@aPD-L1 NBs exhibit significant potential for achieving synergistic anti-cancer effects against PCa (Figure 1).

## Materials and Methods

### Materials

Biotin-poly ethylene glycol distearoylphosphatidylethanolamine2000 (Biotin-DSPE-PEG2000) and disaturated phosphatidyl choline (DPPC) were acquired from Melopeg. Ce6 was obtained from Macklin, 3 $\beta$ [N-(N', N'-dimethylaminoethane)-carbamoyl] cholesterol (DC-chol) from Glpbio, streptavidin (SA) from Solarbio, and biotin-anti-PD-L1 Ab from Thermo Fisher Scientific.

Trichloromethane, PBS, C<sub>3</sub>F<sub>8</sub>, and glycerol were sourced from Servicebio (China).

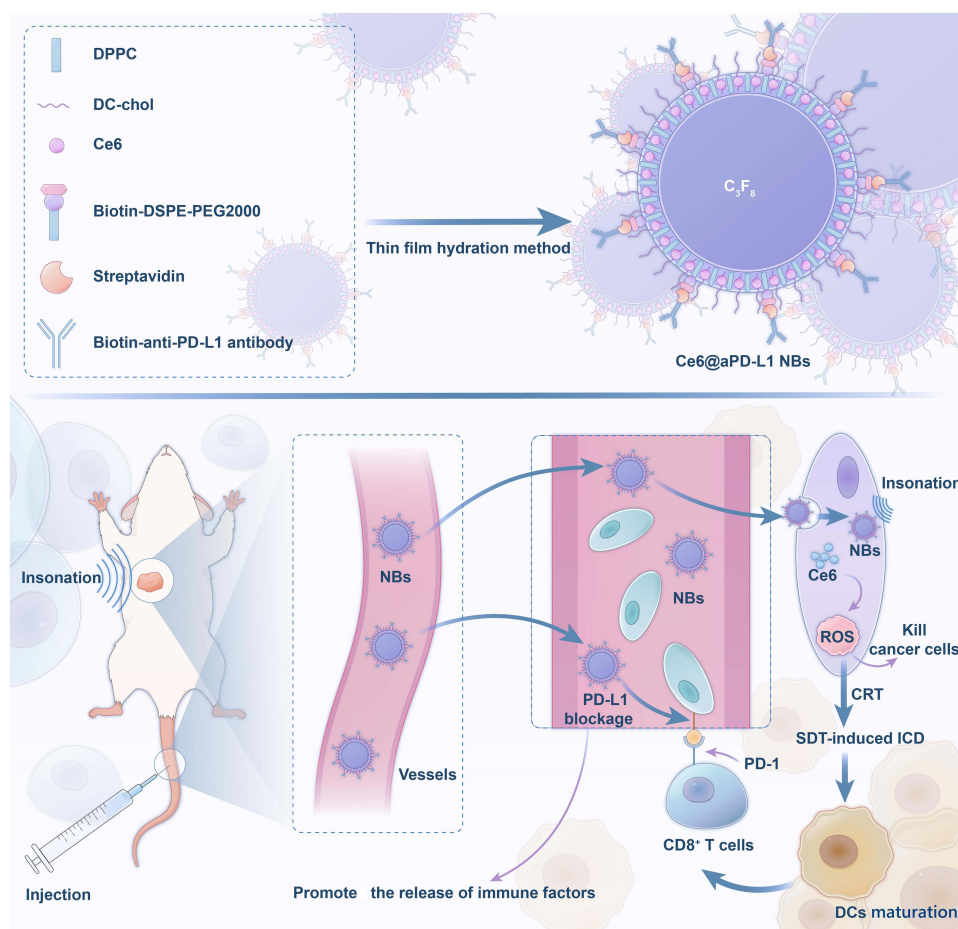


**Figure 1** Illustration diagram of the preparation of Ce6@aPD-L1 NBs and the tumor-targeting immuno-sonodynamic combination therapy for prostate cancer therapy in vivo.

## Preparation of Ce6@aPD-L1 NBs

Ce6@aPD-L1 NBs were synthesized through a thin film hydration method. Initially, a mixture of 31 mg contained DPPC: biotin-DSPE-PEG2000: DC-cholesterol: Ce6 (5:2:0.5:0.25) was dissolved in a glass-bulb tube with trichloromethane. The liquid was evaporated using a rotary evaporator, creating a thin film on the tube wall. Next, 10 mL of glycerol: PBS (1:9) was added, and the tube was shaken in a constant-temperature bath at 45°C for 1 h. Subsequently, 500  $\mu$ L of the liquid was injected into a penicillin bottle with C<sub>3</sub>F<sub>8</sub>, subjected to rapid shake by amalgamator with 1200 rpm for 60s, and then stewed for 5 min to obtain biotin-Ce6-NB suspension. SA: suspension (3:50) was co-incubated at 37°C for 1 h, and biotin-anti-PD-L1 Ab, twice as much as SA, was added to incubate in the refrigerator at 4°C overnight, resulting in the successful preparation of Ce6@aPD-L1 NBs.

## Test for Physical and Chemical Properties of NBs

The size, zeta potential, and particle dispersion index (PDI) of NBs were measured using a Zetasizer.

Nano ZS at 25°C (Malvern, UK). The morphology and distribution of different NBs were observed using optical microscopy, and the red fluorescence of Ce6 was detected using fluorescence microscopy (FSMS). The inspections were conducted at 0, 24, 48, and 96 h, respectively.

## Ce6 and Anti-PD-L1 Ab Loading Test of Ce6@aPD-L1 NBs

Following the synthesis of Ce6@aPD-L1 NBs, a fluorescein isothiocyanate (FITC)-conjugated biotin-anti-PD-L1 antibody was introduced to the NBs and incubated for 1 h at room temperature.

The connectivity of the anti-PD-L1 Ab was assessed using flow cytometry with excitation and emission wavelengths of 488 and 525 nm, respectively. Similarly, Ce6 was analysed using flow cytometry at excitation and emission wavelengths of 638 and 660 nm, respectively.

## Cell Culture

The human PCa cell line PC3, obtained from ProCell (China), was cultured in F12K medium containing 10% fetal bovine serum (FBS, Gibco) and 1% penicillin/streptomycin under a humidified atmosphere of 5% CO<sub>2</sub> at 37°C.

## Cellular Uptake of Ce6

PC3 cells in logarithmic growth phase were inoculated into 12 hole plates, and the cell density of each hole was about 30%. When the cells were in good condition, they were divided into three groups: Ce6@aPD-L1 NBs, Ce6 NBs and free Ce6, each group with three holes. The same content of Ce6 was added to the hole plate and the PC3 cells were treated with ultrasonic irradiation (2 MHz, 1.5 W/cm<sup>2</sup>, 20% duty cycle) for 5 min. Then they were placed in 37 °C 5% CO<sub>2</sub> constant temperature incubator for 12 h. The cells were washed with PBS for three times and stained with diamidino phenylindole (DAPI). Last, the aggregation of Ce6 in cells was observed under FSMS and cellular uptake of Ce6 detected by flow cytometry.

## Detection of ROS Generation

PC3 cells in the logarithmic growth phase were plated into 12-well plates, with each well reaching approximately 30% cell density. Four groups were established: NBs, free Ce6, Ce6 NBs, and Ce6@aPD-L1 NBs, each containing three wells. Subsequently, the cells were placed in a 37 °C 5% CO<sub>2</sub> constant temperature incubator. After 12 h of culturing, each well received 200µL of drugs and was subjected to sonication (2 MHz, 1.5 W/cm<sup>2</sup>, 20% duty cycle) for 5 min. All groups were then exposed to a mixture of DMEM and DCFH-DA at a volume ratio of 1:1000, followed by an additional 30 min incubation at 37 °C. After washing with PBS, fluorescence intensity was measured using a fluorescence microscope (excitation wavelength, 488 nm; emission wavelength, 525 nm). Finally, flow cytometry was employed to determine the number of cells expressing ROS.

## Animal Model

BALB/C-Nude male mice were procured from Beijing Vital River Laboratory Animal Technology Co., Ltd., and all procedures involving animals adhered to the guidelines of the Institutional Animal Care and Use Committee of Wuhan University. A subcutaneous implantation of 1×10<sup>6</sup> PC3 cells in 100 µL of F12K medium without FBS was performed at the dorsal side of the left front leg of 4- to 6-week-old mice to establish the animal tumor model.

## Biodistribution and Pharmacokinetics of Ce6 in vivo

When the tumor diameter reached 5 ± 2 mm, mice (n = 3) were intravenously injected with free Ce6, Ce6 NBs, and Ce6@aPD-L1 NBs (250 µL each) via the tail vein. At 0.5, 1, 6, 12, 24, and 48 h post-injection, the fluorescence signals of the mice were monitored using an in vivo fluorescence imaging instrument (AniView Phoenix, BLT) with an excitation wavelength of 620 nm and an emission wavelength of 670 nm. Tumors and major organs were excised at the time of the strongest fluorescence signals after injection and examined separately using the fluorescence imaging instrument.

## Synergistic Anti-Cancer Effect in vivo

Tumor-bearing mice were randomly allocated into five groups and treated with PBS (control group), Free Ce6 + SDT, Ce6 NBs + SDT, aPD-L1 NBs + SDT, and Ce6@aPD-L1 NBs + SDT. The drug doses for each mouse were 250µL per injection at intervals of 2 days for a total of five times.

When the tumor diameter reached 5 ± 2 mm, mice underwent ultrasonic insonation (2MHz, 1.5 W/cm<sup>2</sup>, 20% duty cycle, 10 min) at 6 h post-administration. Survival rates and body weights of the mice were recorded and plotted against

time. Additionally, tumor volumes were calculated using the formula:  $\text{Volume} = 0.5 \times L \times W^2$ , where L and W represent the length and width of the tumor, respectively.

## Biochemistry Index and Histology Analysis

On day 15 post the initial treatment, the tumor was excised for haematoxylin-eosin staining (HE) to observe alterations in the tumor tissue. The TUNEL immunofluorescence kit was employed to identify apoptotic cells in the tumor tissues. Additionally, real-time fluorescence quantitative polymerase chain reaction (RT-PCR) was conducted to assess the expression of B-cell lymphoma-2 (Bcl-2), Bcl-2 associated x (Bax), interferon- $\gamma$  (IFN- $\gamma$ ), cluster of differentiation 80 (CD80), CD86, transforming growth factor- $\beta$  (TGF- $\beta$ ), and PD-L1. Immunofluorescence staining was utilized to observe the translocation of CRT and the infiltration of CD8+ T cells into the tumor tissue.

## Biosafety Analysis

Following the completion of the treatment, liver functions, including ALT, AST, and TBIL, were assessed. The major organs of the mice were further evaluated by HE staining to observe changes in the tumor tissue structure. Before HE staining, the liver was weighed, and the liver index weight (liver / body weight  $\times$  100%) was calculated for all groups.

## Statistical Analysis

Data are presented as the mean  $\pm$  standard deviation (SD). Statistical analyses were performed conducted using ANOVA with a Tukey's post hoc test. A significance level of  $P < 0.05$  was considered to be statistically significant.

## Results

### Physical and Chemical Properties of Ce6@aPD-L1 NBs

Under an optical microscope, Ce6@aPD-L1 NBs were observed to be spherical, uniform, with no apparent aggregation or clustering. The loading contents of Ce6 and anti-PD-L1 Ab on the Ce6@aPD-L1 NBs were 86.1% and 73.8%, respectively. Within 24 h, all test indices of Ce6@aPD-L1 remained stable. However, after 48 h, changes were noted in the diameter, PDI, Zeta potential, Ce6 and anti-PD-L1 Ab loading rate ( $P < 0.05$ ) (Figure 2).

### Cellular Uptake of Ce6 and SDT Assessments in vitro

After 12 h of culture with drugs, PC3 cells exhibited blue fluorescence in their nuclei and red fluorescence in the cytoplasm when stained with DAPI, confirming the uptake of different Ce6 formulations by the cells. Cellular uptakes of Ce6@aPD-L1 and Ce6 NBs were higher than that of Free Ce6, as observed through FSMS and flow cytometry. Cells treated with NBs showed minimal ROS generation, while ROS levels were detectable in cells treated with different Ce6 formulations, with the Free Ce6 group exhibiting the lowest ROS production (Figures 3 and 4).

### Biodistribution of Ce6 in vivo

After intravenous administration for 12 h, tumors and major organs were excised and monitored using an in vivo fluorescence imaging instrument. Results showed that Free Ce6, Ce6 NBs, and Ce6@aPD-L1 NBs accumulated at tumor sites, with Ce6@aPD-L1 NBs demonstrating more efficient tumor accumulation than the others at all time points. Fluorescence signals in the liver and kidney were also detected, with the Ce6 signal being lower than that in the tumor (Figure 5).

### Synergistic Anticancer Effect of Immunotherapy and SDT

Except for the control group, all other groups exhibited varying degrees of therapeutic effects, with tumor growth inhibited in mice treated with Ce6@aPD-L1 NBs + SDT. On day 15 after the first treatment, the tumor volume in the Ce6@aPD-L1 NBs + SDT group was  $216 \pm 89 \text{ mm}^3$ . In comparison, tumors grew to  $803 \pm 106$ ,  $749 \pm 137$ ,  $337 \pm 126$ , and  $383 \pm 108 \text{ mm}^3$  in the control, Free Ce6 + SDT, Ce6 NBs + SDT, and aPD-L1 NBs + SDT groups, respectively (Figure 6A and B).

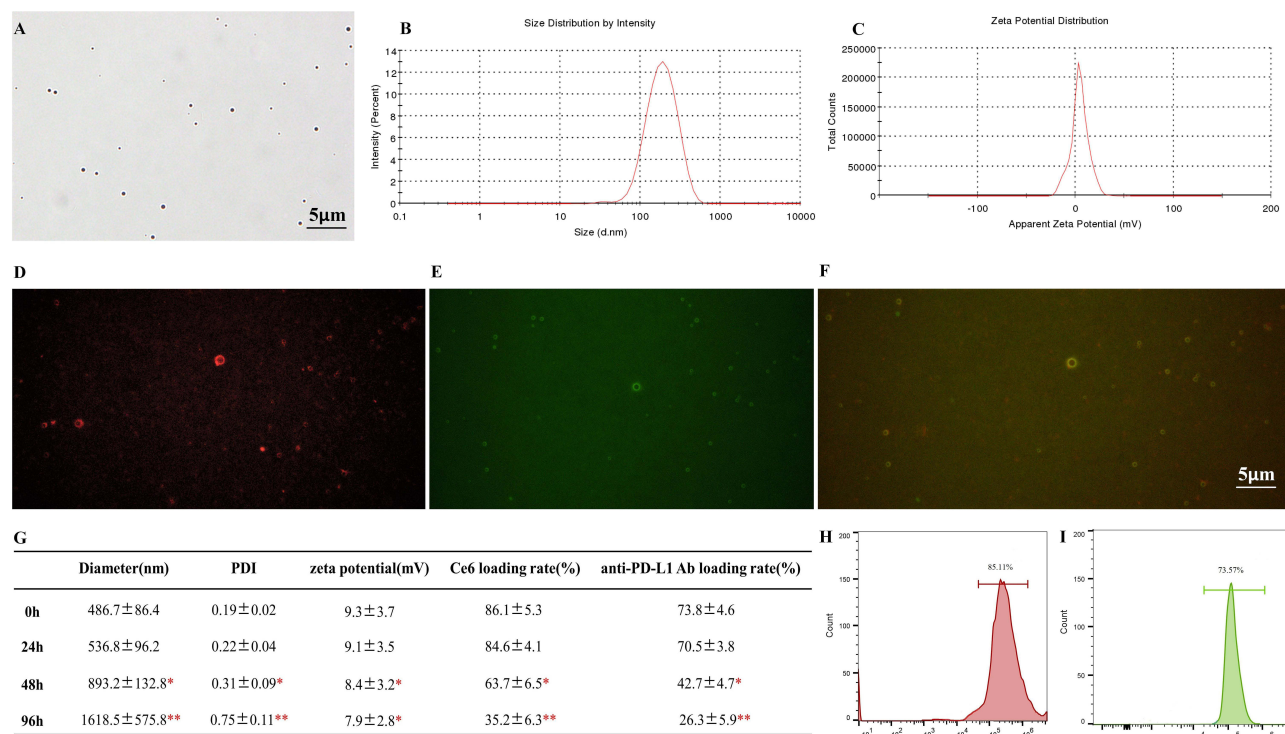


**Figure 2** Characterization of Ce6@aPD-L1 NBs. (A) The morphology of Ce6@aPD-L1 NBs observed under optical microscope, Scale bar = 5 $\mu$ m. (B and C) The size and zeta potential of Ce6@aPD-L1 NBs detected by Zetasizer Nano ZS. (D–F) The fluorescence signal of Ce6@aPD-L1 NBs under FSMS: red fluorescence signal of Ce6, green fluorescence signal of FITC marked with anti-PD-L1 Ab, and the red and green fluorescence signal were completely coincident. Scale bar = 5 $\mu$ m. (G) With the time prolonging, the size and PDI were increasing, while the zeta potential, Ce6 and anti-PD-L1 Ab loading rate of Ce6@aPD-L1 NBs were decreasing. (H and I) The Ce6 and anti-PD-L1 Ab loading rate of Ce6@aPD-L1 NBs were tested by flow cytometry. \* $P < 0.05$  \*\* $P < 0.01$ .

Consistent with the tumor growth inhibition results, Ce6@aPD-L1 NBs + SDT most effectively prolonged the survival rate of mice (Figure 6C). The rate of body weight gain in the control and Free Ce6 + SDT groups decreased gradually, whereas that in the other groups increased (Figure 6D).

Tumor tissues from animals treated with PBS were hypercellular. In contrast, the cancer cell density in tumor tissues from animals receiving Ce6 NBs + SDT, aPD-L1 NBs + SDT, and Ce6@aPD-L1 NBs + SDT decreased. Moreover, the TUNEL assay showed that the tumor tissue of the Ce6@aPD-L1 NBs + SDT group exhibited the most significant apoptosis (Figure 7A). Compared with the control group, the BAX expression level was up-regulated, and the group of Ce6@aPD-L1 NBs + SDT showed the most significant increase ( $P < 0.01$ ). Conversely, BCL2 was downregulated, with the group of Ce6@aPD-L1 NBs + SDT also showing the most significant decrease ( $P < 0.01$ ) (Figure 7B and C).

Immunofluorescence staining demonstrated that compared to the rare tumor infiltration of CD8+ T cells in the group, tumor infiltration of CD8+ T cells increased with treatment using other drugs. Particularly, Ce6@aPD-L1 NBs + SDT promoted tumor infiltration of CD8+ T cells (Figure 8A). During aPD-L1 NBs + SDT and Ce6@aPD-L1 NBs + SDT, the CD80, CD86, and IFN- $\gamma$  expression levels were significantly up-regulated ( $P < 0.01$ ), while the TGF- $\beta$  expression level was significantly down-regulated ( $P < 0.01$ ). Similarly, the PD-L1 expression level was downregulated in the aPD-L1 NBs + SDT and Ce6@aPD-L1 NBs + SDT groups ( $P < 0.05$ ) (Figure 8B).

Immunofluorescent staining revealed that the CRT fluorescence signal in the tumor tissue was marginal in the control and aPD-L1 NBs + SDT groups. In comparison, the Ce6 NBs + SDT and Ce6@aPD-L1 NBs + SDT groups exhibited the most significant increase (Figure 9).

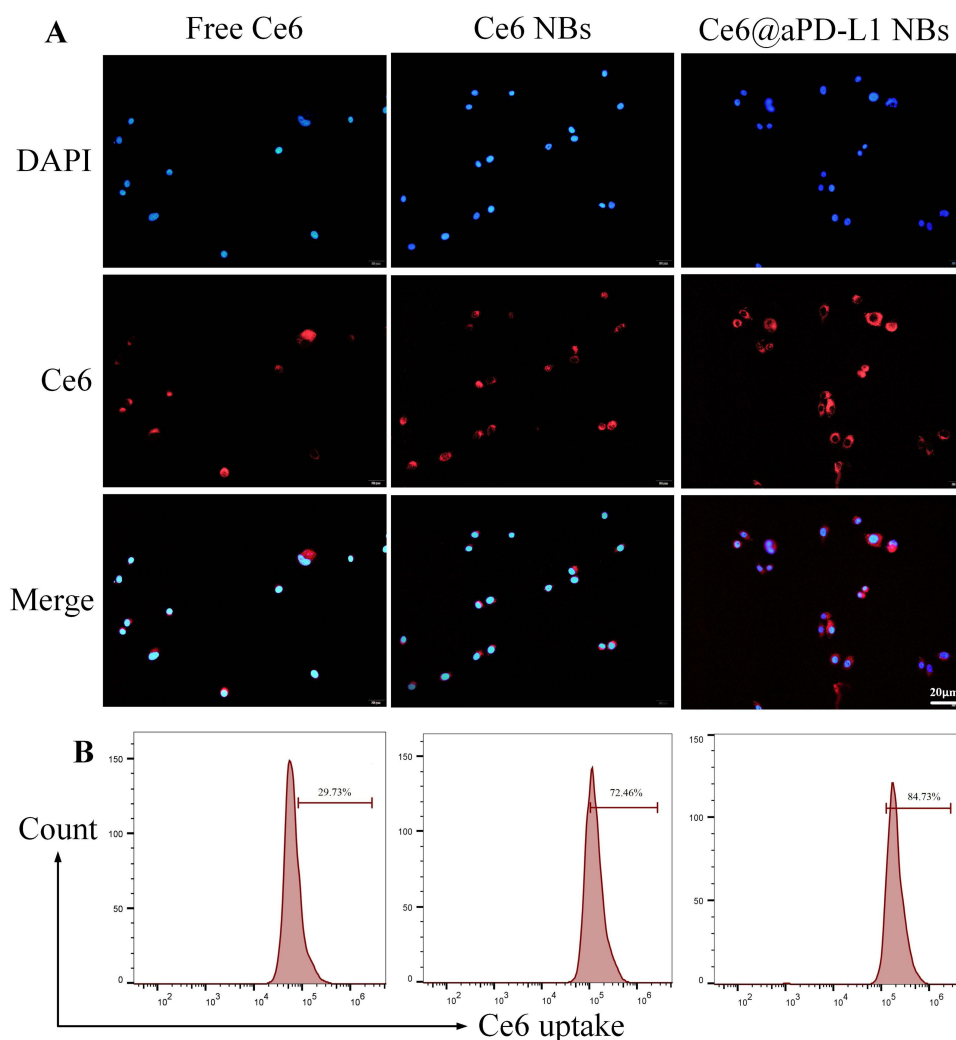


**Figure 3** Cellular uptake of Ce6. Different formulation of Ce6 were detected in PC3 cells after treating with ultrasonic irradiation, and the cellular uptake of Ce6 was detected by FSMS (A) and flow cytometry (B). Scale bar = 20µm.

## Biosafety Analysis of Therapy

According to the results of HE staining, no apparent histological damage was observed in the heart, liver, spleen, lungs, and kidneys in all groups. Additionally, levels of ALT, AST, and TBIL were within normal range ( $P>0.05$ ). Likewise, There were no significant differences of the liver index among the groups ( $P>0.05$ ) (Figure 10).

## Discussion

Cancer-targeted therapy, focusing on treating specific carcinoma sites at the cellular level, has garnered increasing attention from researchers. Immunotherapy, a promising approach to targeted therapy,<sup>24</sup> can be used alone or in combination with chemotherapy, radiotherapy, or surgery. The anti-PD-L1 Ab, a representative type of ICB, has been widely applied in experimental research and clinical treatment.<sup>25</sup> Due to the complex composition of TME,<sup>26</sup> a sole application of ICB may not effectively activate the immune system.<sup>27</sup> Therefore, we developed SDT, a non-invasive therapeutic modality combining low-intensity US and sonosensitisers.<sup>28</sup>

The simultaneous achievement of immunotherapy and SDT anti-cancer effects is crucial. Ce6, a representative and promising sonosensitiser, is a stable degradation product of chlorophyll a and contains four pyrrole ring structures. Ce6 is non-toxic, exhibits good specificity and fast metabolism, and is not easily soluble in water.<sup>17,19</sup> Therefore, it is necessary to modify free Ce6 using nanotechnology to improve its tissue selectivity, lipophilicity, and ability to bind to NBs with

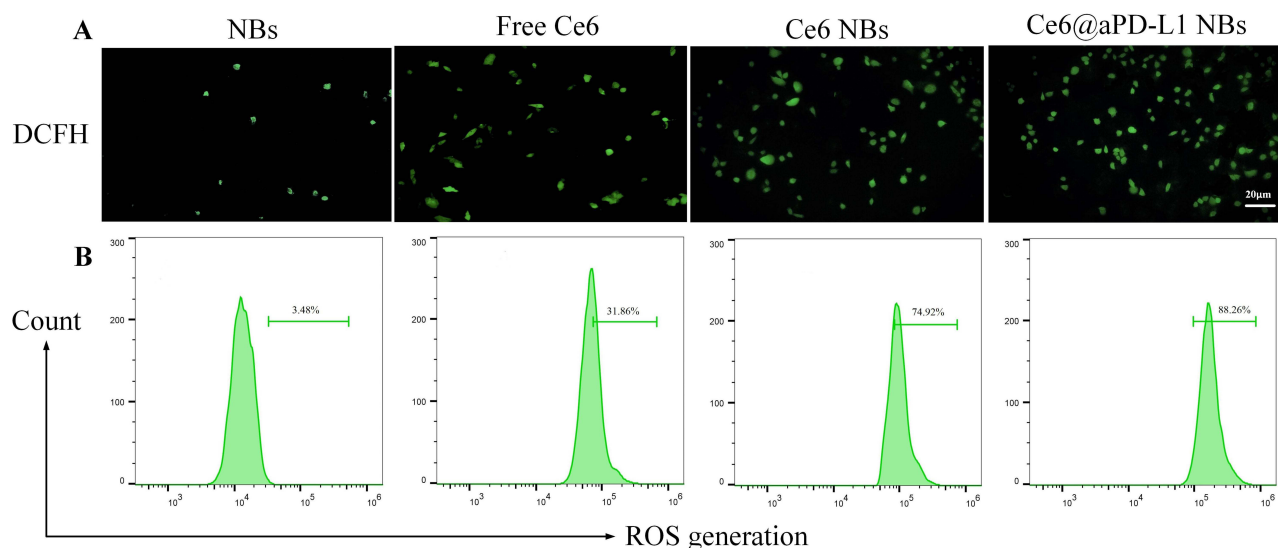


**Figure 4** Generation of ROS in PC3 cells. After cellular uptake of Ce6 and ultrasonic irradiation, the generation of ROS in cells were detected by FSMS (A) and flow cytometry (B). Scale bar = 20 $\mu$ m.

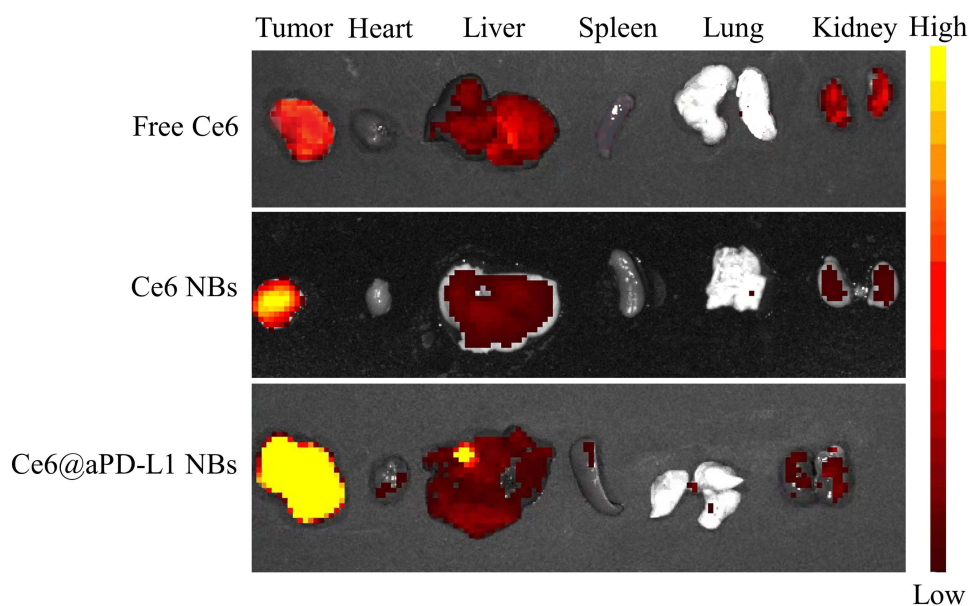


**Figure 5** Biodistribution of Ce6 in vivo. After injecting drugs into the PCa-bearing mice for 12 hours, the tumors and major organs were detected with different intensity signal.

lipid components on the surface. In this study, Ce6@aPD-L1 NBs were successfully synthesized according to a specific route. Firstly, the Ce6 loading rate of NBs was  $86.1 \pm 5.3\%$  and  $84.6 \pm 4.1\%$  at 0 and 24 h, respectively, illustrating that Ce6@aPD-L1 NBs could carry sufficient quantities of Ce6 to ensure the effectiveness of SDT. Secondly, Ce6@aPD-L1 NBs exhibited much more efficient accumulation in the PC3 tumors of mice than free Ce6 and Ce6 NBs, and also more than in the liver and kidneys, confirming the SDT effect.

The particle size of the Ce6@aPD-L1 NBs was uniform at the nanoscale, with no obvious aggregation or clustering. The diameter, PDI, Zeta potential, Ce6, and anti-PD-L1 Ab loading rate remained nearly constant within 24 h, whereas the test indices of the NBs changed after 48 h. Within the first 24 h, the particle size of NBs was approximately 500 nm, enabling them to pass through the endothelial gap of tumor blood vessels, allowing the NBs to enter the tumor tissue

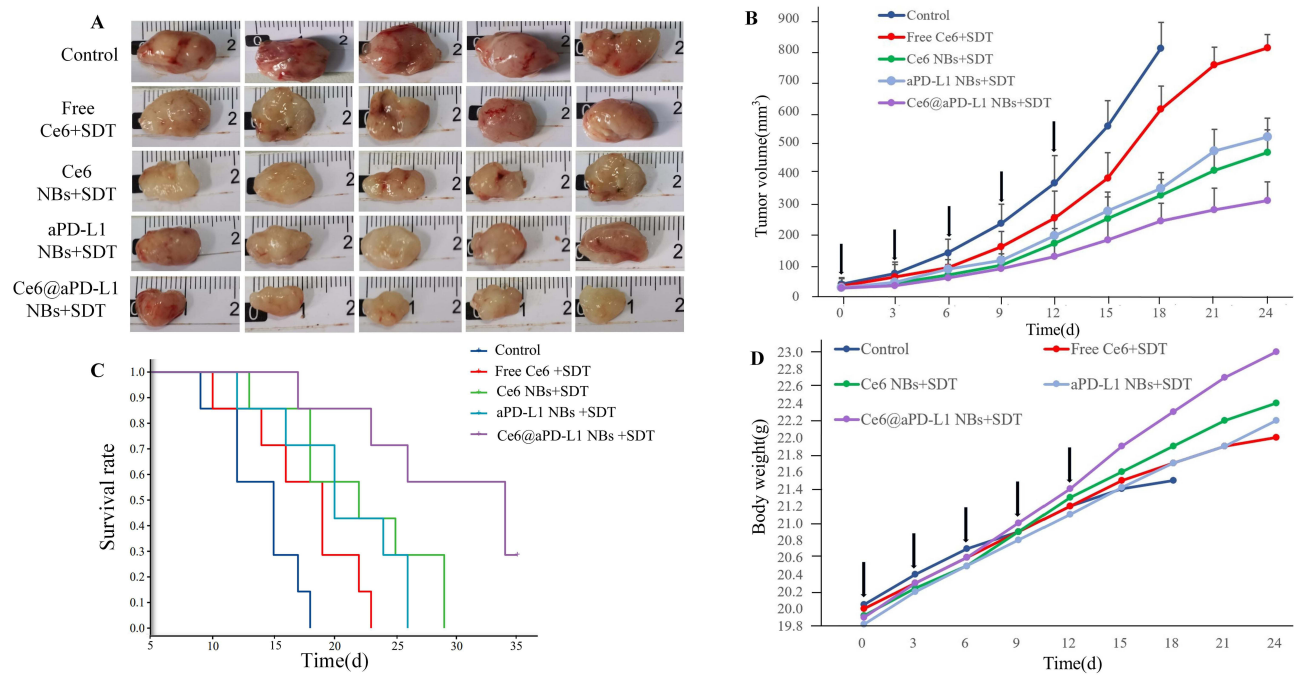


**Figure 6** Assessment of the overall therapeutic effect. **(A)** The images of solid tumors excised. **(B)** The tumor growth of PCa-bearing mice with different drugs for 5 times, as indicated by the black arrows. **(C)** The cumulative survivals of PCa-bearing mice receiving different treatments. **(D)** Body weight change graph of mice after treatment with different drugs for 5 times, as indicated by the black arrows.

through EPR, thus, passively targeting tumor cells. The anti-PD-L1 Ab on Ce6@aPD-L1 NBs was successfully detected by FSMS and flow cytometry, confirming its successful connection to the NBs and its ability to actively target tumor cells. Moreover, the positively charged surface of NBs facilitated their entry into negatively charged tumor tissue.<sup>29</sup>

When PC3 cells that had internalised Ce6 were exposed to US, the production of ROS in the cells was assessed through FSMS and flow cytometry. ROS generation primarily depends on the synergistic interactions of US, a non-toxic photosensitizer,<sup>30</sup> and molecular oxygen, leading to cellular toxicity and apoptosis. Furthermore, following incubation with different drugs, cells from the Ce6@aPD-L1 NBs and Ce6 NBs groups exhibited higher Ce6 uptake compared to free Ce6. Additionally, these groups showed an increased generation of ROS with SDT. Based on these findings, a nanotechnology-assisted combination may enhance SDT efficiency, offering a potentially safer therapeutic option for PCa.

SDT can result in extensive tumor cell death,<sup>31</sup> which includes the direct cytotoxicity of ROS and the cavitation effect of SDT,<sup>32,33</sup> which Bilmin has summarized the sono-mechanical changes caused by the oscillations and fast movement of NBs.<sup>34</sup> During tumor progression, cellular immunity is suppressed, and reactivating immunity may contribute to tumor growth inhibition, so the regulation of the TME is crucial for inhibiting tumor cell growth.<sup>35</sup> SDT can induce ICD in tumor cells, triggering an anti-tumor immune response,<sup>36</sup> and the translocation of CRT to the cell surface is a characteristic feature of ICD. In our study, immunofluorescent staining revealed that the CRT fluorescence signal was not observed in the control and aPD-L1 NBs + SDT groups, while abundant CRT was detected in the Ce6 NBs + SDT and Ce6@aPD-L1 NBs + SDT groups, indicating a successful triggering of the ICD reaction.

Recent studies have suggested that SDT may stimulate the release of certain tumor immune factors, including CD80, CD86, IFN- $\gamma$ , TGF- $\beta$ , IL2, and IL10. PCR results demonstrated that the expression levels of CD80 and CD86—markers related to the maturation of DCs—increased significantly in the tumor tissue of the Ce6 NBs, aPD-L1 NBs, and Ce6@aPD-L1 NBs group. SDT can induce the upregulation of DCs and enhance anti-tumor immune effects.<sup>37</sup> IFN- $\gamma$ , associated with T lymphocyte infiltration in tumor tissue, exhibited increased expression. In contrast, TGF- $\beta$ , an immune suppressive factor, displayed downregulated expression, promoting anti-tumor immune effects. The PD-1/PD-L1 signaling pathway inhibits T cell activation and may lead to apoptosis, influencing tumor immune escape.<sup>38,39</sup> Anti-PD-L1 Ab can specifically bind to the PD-L1 of tumor cells, reactivating and proliferating T cells to enhance anti-tumor immunity.<sup>40</sup>

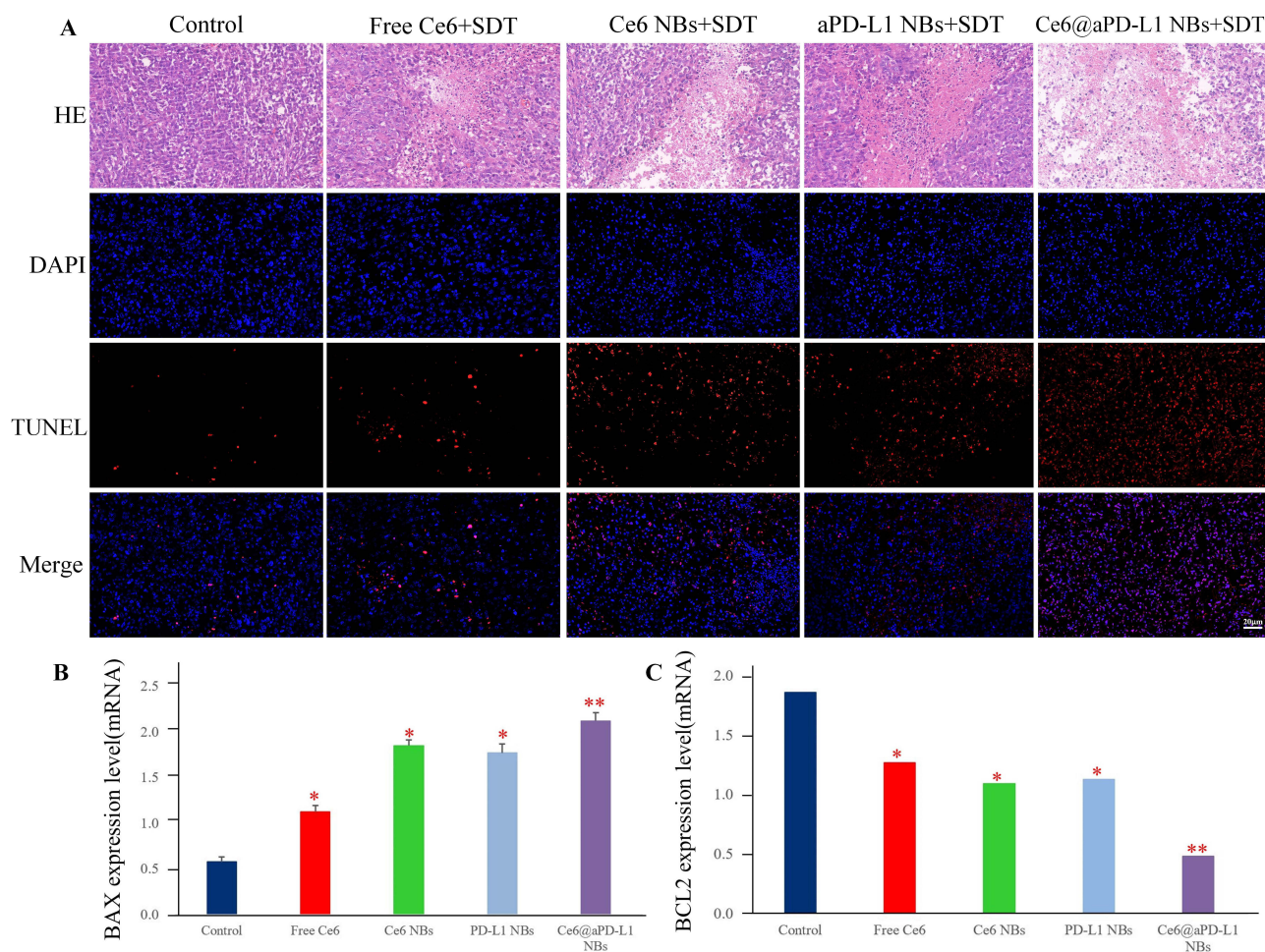


**Figure 7** Assessment of the tumor cell apoptosis. **(A)** The HE and TUNEL test of tumors. Scale bar = 20 $\mu$ m. **(B and C)** The PCR results of BAX and BCL2. \* $P < 0.05$ , \*\* $P < 0.01$ .

The results indicated a significant decrease in the expression of PD-L1 in the aPD-L1 NBs and Ce6@aPD-L1 NBs, accompanied by evident infiltration of CD8<sup>+</sup> T cells into the tumor tissue, suggesting the reactivation of anti-tumor immunity.

After treating mice with PCa, various groups exhibited varying therapeutic effects, with tumor growth inhibition observed in mice treated with Ce6@aPD-L1 NBs + SDT, except for the control group. On day 15 after the initial treatment, the tumor volume in the Ce6@aPD-L1 NBs + SDT group was  $216 \pm 89$  mm<sup>3</sup>, while tumors in the control group grew to  $803 \pm 106$  mm<sup>3</sup>. Consistent with the tumor growth inhibition results, Ce6@aPD-L1 NBs + SDT significantly extended the survival of mice. The rate of body weight growth in the control and Free Ce6 + SDT groups decreased gradually, whereas the other groups exhibited an upward trend, possibly due to the inhibition of tumor growth with less impact on the mice's overall growth. And we observed that the tumor tissues from animals treated with PBS were hypercellular. In contrast, the cancer cell density in tumor tissues from Ce6 NBs + SDT, aPD-L1 NBs + SDT, and Ce6@aPD-L1 NBs + SDT mice clearly declined. Moreover, the TUNEL assay revealed abundant apoptosis in the tumor tissue of the Ce6@aPD-L1 NBs + SDT group. Compared with the control group, the BAX expression level was upregulated, with the most significant upregulation observed in Ce6@aPD-L1 NBs + SDT. Conversely, BCL2 downregulation in the Ce6@aPD-L1 NBs + SDT group was the most significant.

NBs, as a type of liposomes, have been developed as novel ultrasound contrast agents to improve diagnostic accuracy and reliability,<sup>41</sup> and they have smaller particle size, more stable performance, and longer circulation time than MBs, which leads to more accumulation in the tumor area.<sup>42</sup> Through binding drugs to the shells or specific ligands, NBs can serve as a multifunctional platform to deliver drugs, increase local drug concentration, control drug release, and achieve treatment of cancer. Recently, nanotechnology development has implemented carrying multiple medications, and NBs

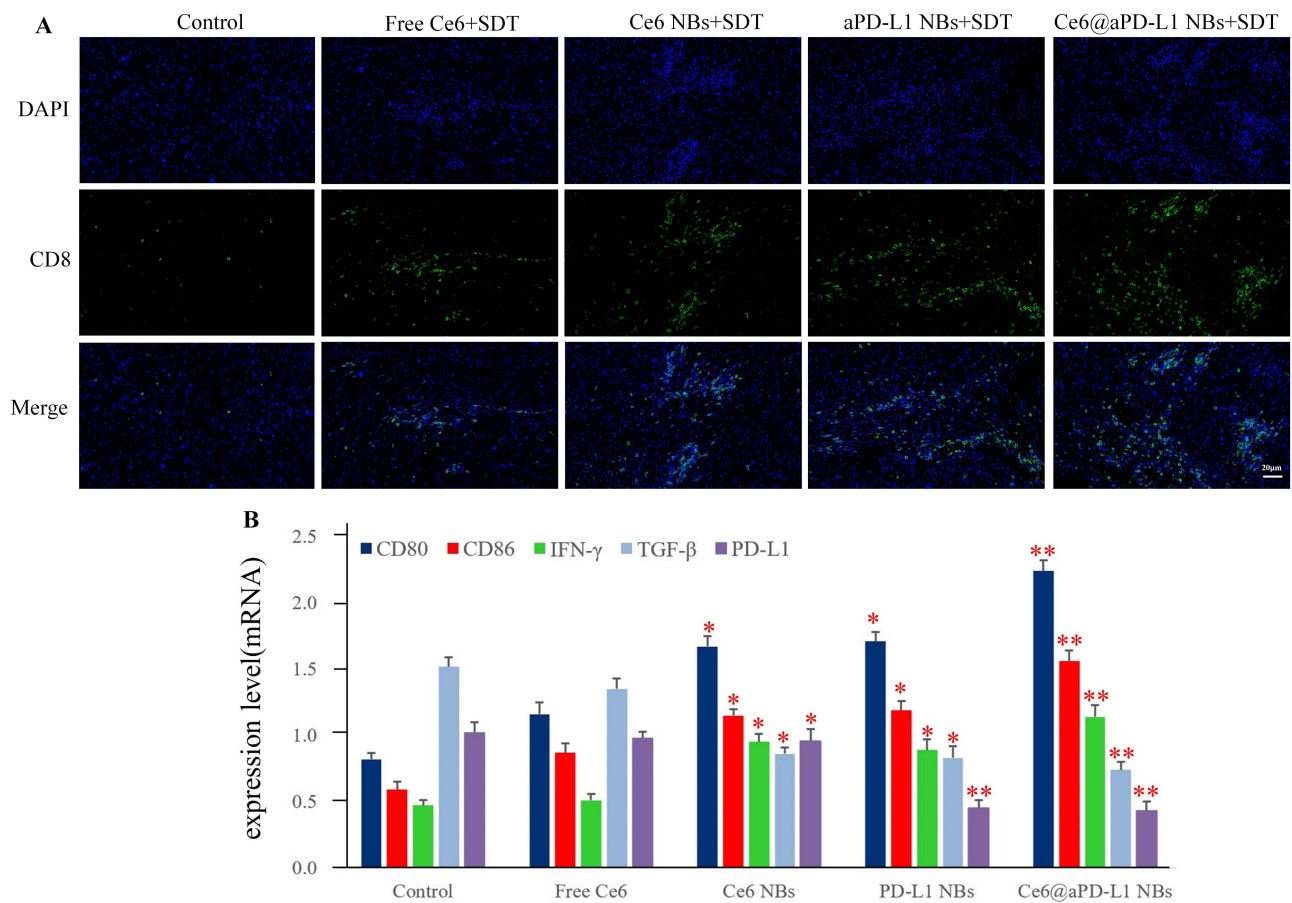


**Figure 8** Tumor immune response in vivo. **(A)** The tumor infiltration of CD8+ T cells by immunofluorescent staining. Scale bar = 20 $\mu$ m. **(B)** The PCR results of CD80, CD86, IFN- $\gamma$ , TGF- $\beta$  and PD-L1. \* $P$  < 0.05, \*\* $P$  < 0.01.

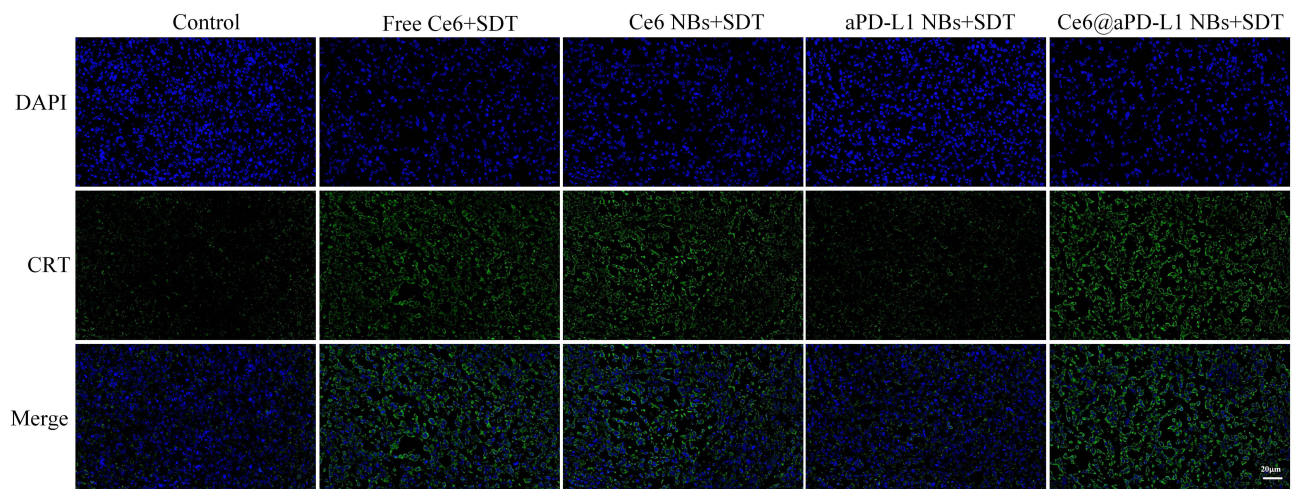


**Figure 9** Analysis of CRT exposure in tumor by immunofluorescent staining. Compared with the control and aPD-L1 NBs + SDT group, CRT fluorescence signal in tumor tissue was amplified significantly. Scale bar = 20 $\mu$ m.

loaded with Ce6 make SDT potentially a safe and feasible therapeutic means for various tumors.<sup>43</sup> On the other hand, SDT was reported to induce acute inflammation which promotes lymphocytes infiltration in tumor, thus triggering an anti-tumor immunity.<sup>35</sup>

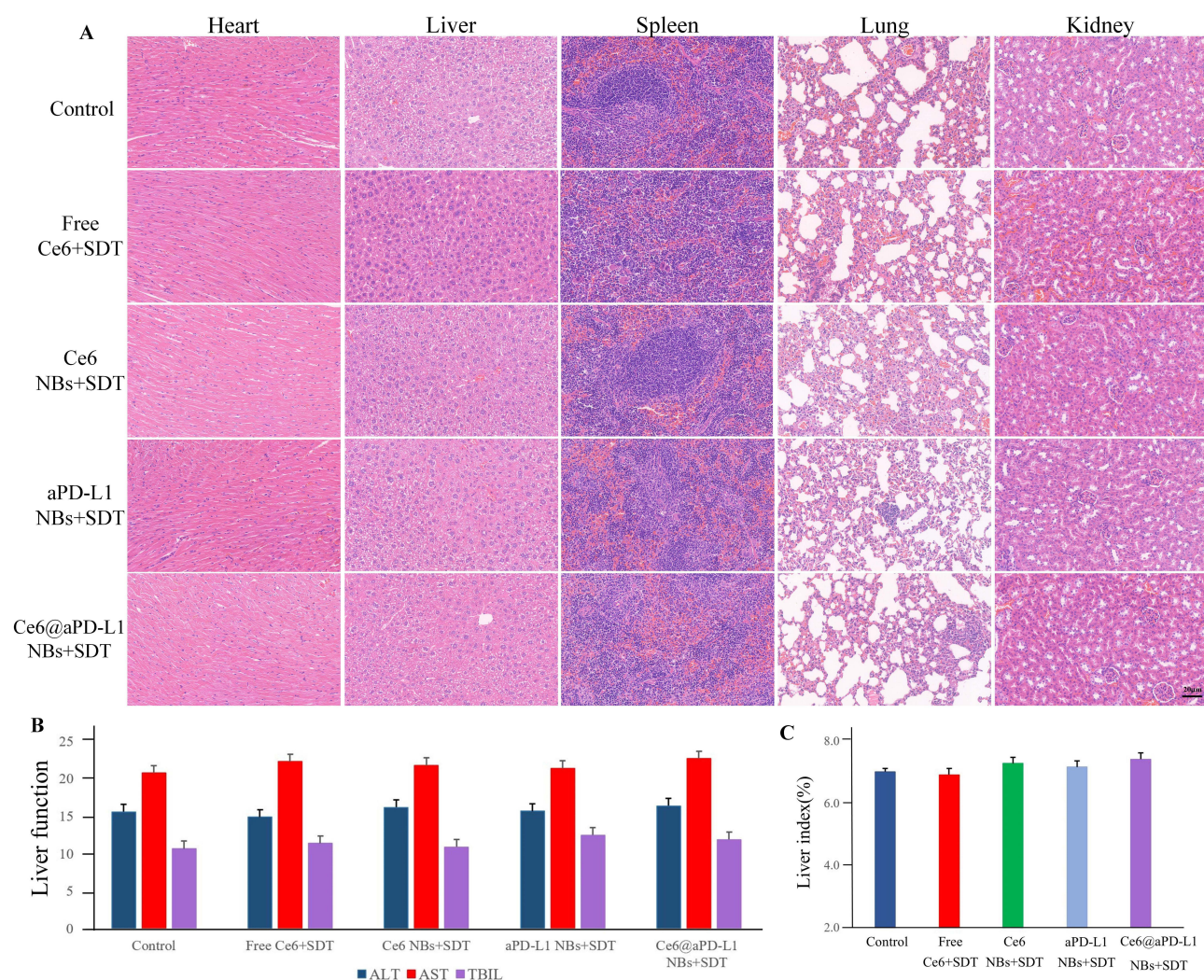


**Figure 10** Biosafety evaluation of mice in vivo. **(A)** The HE staining of major organs (heart, liver, spleen, lung, kidney) treated with different drug groups. Scale bar = 20 $\mu$ m. **(B)** The blood biochemical indexes of hepatic (ALT, AST and TBL). **(C)** The liver index of different drug groups.

## Conclusion

In summary, we successfully developed effective NBs co-loaded with anti-PD-L1 Ab and Ce6 for treating PCa tumors. These NBs can effectively inhibit tumor growth not only due to the direct action of SDT but also because of the reactivation of the immune system, enhancing immune responses in the TME. Synergetic immunotherapy may involve ICD induced by SDT and ICB of PD-1/PD-L1, including the translocation of CRT to the tumor cell surface, release of tumor immune factors, activated maturation of DCs, and effective stimulation of CD8<sup>+</sup> T cells. The promising Ce6@aPD-L1 NBs holds great potentials for achieving synergetic anti-cancer effect for PCa, but also can be applied in the treatment of other solid tumors.

## Ethics Approval

This experiment was performed according to the Animal Ethics Committee of Renmin Hospital of Wuhan University (IACUC Issue No.20201103). In this study, we adhered to the ARRIVE guidelines and strictly followed the Regulations of the People's Republic of China on the Administration of Laboratory Animals and its guiding principles for animal experiments. Our approach fully respected the lives of laboratory animals and aimed to minimize their suffering.

## Acknowledgments

The authors greatly appreciated the support from the Central Laboratory and Animal Experiment Center of Renmin hospital of Wuhan University. This work was sponsored by the National Natural Science Foundation of China [Grant numbers 82271999].

## Author Contributions

All authors made a significant contribution to the work reported, whether that is in the conception, study design, execution, acquisition of data, analysis and interpretation, or in all these areas; took part in drafting, revising or critically reviewing the article; gave final approval of the version to be published; have agreed on the journal to which the article has been submitted; and agree to be accountable for all aspects of the work.

## Disclosure

The authors report no conflicts of interest in this work.

## References

1. Ferlay J, Colombet M, Soerjomataram I, et al. Cancer statistics for the year 2020: an overview. *Int J Cancer*. 2021;149:778–789. doi:10.1002/ijc.33588
2. Martel CL, Gumerlock PH, Meyers FJ, Lara PN. Current strategies in the management of hormone refractory prostate cancer. *Cancer Treat Rev*. 2003;29(3):171–187. doi:10.1016/S0305-7372(02)00090-7
3. Tannock IF, Wit RD, Berry WR, et al. Docetaxel plus prednisone or mitoxantrone plus prednisone for advanced prostate cancer. *N Engl J Med*. 2004;351:1502–1512. doi:10.1056/NEJMoa040720
4. Clarke NW, Ali A, Ingleby FC, Hoyle A, James ND. Addition of docetaxel to hormonal therapy in low-and high-burden metastatic hormone sensitive prostate cancer: long-term survival results from the stampede trial. *Ann Oncol*. 2019;30(12):1992–2003. doi:10.1016/j.annonc.2020.01.002
5. Gravis G, Audenet F, Irani J, Timsit M, Barthelemy P. Chemotherapy in hormone-sensitive metastatic prostate cancer: evidences and uncertainties from the literature. *Cancer Treat Rev*. 2017;55:211–217. doi:10.1016/j.ctrv.2016.09.008
6. Ioannides CG, Whiteside TL. T cell recognition of human tumors: implications for molecular immunotherapy of cancer. *Clin Immunol Immunopathol*. 1993;66(2):91–106. doi:10.1006/clin.1993.1012
7. Taube JM, Klein A, Brahmer JR, et al. Association of PD-1, PD-1 ligands and other features of the tumor immune microenvironment with response to anti-PD-1 therapy. *Clin Cancer Res*. 2014;20(19):5064–5074. doi:10.1158/1078-0432.CCR-13-3271
8. Topalian SL, Drake CG, Pardoll DM. Targeting the PD-1/B7-H1(PD-L1) pathway to activate anti-tumor immunity. *Curr Opin Immunol*. 2012;24(2):207–212. doi:10.1016/j.coi.2011.12.009
9. Darvin P, Toor SM, Nair VS, Elkord E. Affiliations expand immune checkpoint inhibitors: recent progress and potential biomarkers. *Exp Mol Med*. 2018;50(12):1–11. doi:10.1038/s12276-018-0191-1
10. Puzanov I, Diab A, Abdallah K, et al. Managing toxicities associated with immune checkpoint inhibitors: consensus recommendations from the society for immunotherapy of cancer(SITC) toxicity management working group. *J Immunother Cancer*. 2017;5(1):95–123. doi:10.1186/s40425-017-0300-z
11. Soularue E, Lepage P, Colombel JF, et al. Enterocolitis due to immune checkpoint inhibitors: a systematic review. *Gut*. 2018;67(11):2056–2067. doi:10.1136/gutjnl-2018-316948
12. Boissenot T, Bordat A, Fattal E, Tsapis N. Ultrasound-triggered drug delivery for cancer treatment using drug delivery systems: from theoretical considerations to practical applications. *J Control Release*. 2016;241:144–163. doi:10.1016/j.jconrel.2016.09.026
13. Thakur SS, Chen YS, Houston ZH, et al. Ultrasound-responsive nanobubbles for enhanced intravitreal drug migration: an ex vivo evaluation. *Eur J Biopharm*. 2019;136:102–107. doi:10.1016/j.ejpb.2019.01.014
14. Prokhnevskaya N, Emerson DA, Kissick HT, Redmond WL. Immunological complexity of the prostate cancer microenvironment influences the response to immunotherapy. *Adv Exp Med Biol*. 2019;1210:121–147. doi:10.1007/978-3-030-32656-2\_7
15. Trendowski M. The promise of sonodynamic therapy: using ultrasonic irradiation and chemotherapeutic agents as a treatment modality. *J Cancer Sci Ther*. 2014;6:10. doi:10.4172/1948-5956.S1.03
16. Chen H, Hwang JH. Ultrasound-targeted microbubble destruction for chemotherapeutic drug delivery to solid tumors. *J Ther Ultr*. 2013;1(1):10. doi:10.1186/2050-5736-1-10
17. Lin X, Song J, Chen X, Yang H. Ultrasound-activated sensitizers and applications. *Angew Chem Int Ed*. 2020;59(34):14212–14233. doi:10.1002/anie.201906823
18. Li D, Yang Y, Li D, Pan J, Chu C, Liu G. Organic sonosensitizers for sonodynamic therapy: from small molecules and nanoparticles toward clinical development. *Small*. 2021;17(42):e2101976. doi:10.1002/smll.202101976
19. Huang JS, Xiao ZC, An YC, et al. Nanodrug with dual-sensitivity to tumor microenvironment for immuno-sonodynamic anti-cancer therapy. *Biomaterials*. 2021;269:120636. doi:10.1016/j.biomaterials.2020.120636
20. Chen W, Schilperoord M, Cao Y, Shi J, Tabas I, Tao W. Macrophage-targeted nanomedicine for the diagnosis and treatment of atherosclerosis. *Nat Rev Cardiol*. 2022;19:228–249. doi:10.1038/s41569-021-00629-x
21. Ma Y, Li JL, Zhao Y, Hu B, Liu Y, Liu CQ. Nanobubble-mediated co-delivery of Ce6 and miR-195 for synergized sonodynamic and checkpoint blockade combination therapy with elicitation of robust immune response in hepatocellular carcinoma. *Eur J Pharm Biopharm*. 2022;181:36–48. doi:10.1016/j.ejpb.2022.10.017

22. Diamandis EP, Christopoulos TK. The biotin-(strept) avidin system: principles and applications in biotechnology. *Clin Chem*. 1991;37(5):625–636. doi:10.1016/0009-8981(91)90363-H
23. Perera RH, Leon DA, Wang X, et al. Real time ultrasound molecular imaging of prostate cancer with PSMA-targeted nanobubbles. *Nanomedicine*. 2020;28:102213. doi:10.1016/j.nano.2020.102213
24. Riley RS, June CH, Langer R, Mitchell MJ. Delivery technologies for cancer immunotherapy. *Nat Rev Drug Discov*. 2019;18(3):175–196. doi:10.1038/s41573-018-0006-z
25. Bolat D, Haydarolu A. Immunotherapy in Prostate Cancer. *Bull Urooncol*. 2019;18(2):67–72. doi:10.4274/uob.galenos.2018.1142
26. Shiao SL, Chu CY, Chung LW. Regulation of prostate cancer progression by the tumor microenvironment. *Cancer LettNE*. 2016;380(1):340–348. doi:10.1016/j.canlet.2015.12.022
27. Graff JN, Alumkal JJ, Drake CG, Thomas GV, Beer TM. Early evidence of anti-PD-1 activity in enzalutamide-resistant prostate cancer. *Oncotarget*. 2016;12(33):52810–52817. doi:10.18632/oncotarget.10547
28. Son S, Kim JH, Wang X, et al. Multifunctional sonosensitizers in sonodynamic cancer therapy. *Chem Soc Rev*. 2020;49(11):3244–3261. doi:10.1039/C9CS00648F
29. Li P, Liu Y, Liu W, et al. IR-783 inhibits breast cancer cell proliferation and migration by inducing mitochondrial fission. *Int J Oncol*. 2019;55(2):415–424. doi:10.3892/ijo.2019.4821
30. Chen HJ, Zhou XB, Gao Y, Zheng BY, Tang FX, Huang JD. Recent progress in development of new sonosensitizers for sonodynamic cancer therapy. *Drug Discov Today*. 2014;19(4):502–509. doi:10.1016/j.drudis.2014.01.010
31. Zhao P, Deng Y, Xiang G, Liu Y. Nanoparticle-assisted sonosensitizers and their biomedical Applications. *Int J Nanomedicine*. 2021;16(6):4615–4630. doi:10.2147/IJN.S307885
32. Ibsen S, Schutt CE, Esener S. Microbubble-mediated ultrasound therapy: a review of its potential in cancer treatment. *Drug Des Devel Ther*. 2013;7::375–388. doi:10.2147/DDDT.S31564
33. Tu J, Zhang H, Yu J, Liu FC, Chen Z. Ultrasound-mediated microbubble destruction: a new method in cancer immunotherapy. *Oncol Targets Ther*. 2018;11:5763–5775. doi:10.2147/OTT.S171019
34. Bilmin K, Kujawska T, Grieb P. Sonodynamic therapy for gliomas. perspectives and prospects of selective sonosensitization of glioma cells. *Cells*. 2019;8(11):1428. doi:10.3390/cells8111428
35. Yue W, Chen L, Yu L, et al. Checkpoint blockade and nanosonosensitizer-augmented Non-invasive sonodynamic therapy combination reduces tumour growth and metastases in mice. *Nat Commun*. 2019;10(1):2025. doi:10.1038/s41467-019-09760-3
36. Cheng D, Wang X, Zhou X, Li J. Nanosonosensitizers with ultrasound-induced reactive oxygen species generation for cancer sonodynamic immunotherapy. *Front Bioeng Biotechnol*. 2021;30:761218. doi:10.3389/fbioe.2021.761218
37. Zhao H, Zhao B, Li L, et al. Biomimetic decoy inhibits tumor growth and lung metastasis by reversing the drawbacks of sonodynamic therapy. *Adv Healthc Mater*. 2020;9(1):e1901335. doi:10.1002/adhm.201901335
38. Li K, Tian H. Development of small-molecule immune checkpoint inhibitors of PD-1/PD-L1 as a new therapeutic strategy for tumour immunotherapy. *J Drug Target*. 2019;27(3):244–256. doi:10.1080/1061186X.2018.1440400
39. Keir M, Butte M, Freeman G, Sharpe AH. Sharpe A.PD-1 and its ligands in tolerance and immunity. *Annu Rev Immuno*. 2008;26:677–704. doi:10.1146/annurev.immunol.26.021607.090331
40. Robert C, Ribas A, Wolchok JD, et al. Anti-programmed-death-receptor-1 treatment with pembrolizumab in ipilimumab-refractory advanced melanoma: a randomized dose-comparison cohort of a Phase 1 trial. *Lancet*. 2014;384(9948):1109–1117. doi:10.1016/S0140-6736(14)60958-2
41. Wheatley MA, Forsberg F, Dube N, Patel M, Oeffinger BE. Surfactant-stabilized contrast agent on the nanoscale for diagnostic ultrasound imaging. *Ultrasound Med Biol*. 2006;32(1):83–93. doi:10.1016/j.ultrasmedbio.2005.08.009
42. Yang H, Cai W, Xu L, et al. Nanobubble-affibody: novel ultrasound contrast agents for targeted molecular ultrasound imaging of tumor. *Biomaterials*. 2015;37:279–288. doi:10.1016/j.biomaterials.2014.10.013
43. Jiang OY, Zhong MT, Nika F, et al. Ultrasound mediated therapy: recent progress and challenges in nanoscience. *Nano Today*. 2020;35:100949. doi:10.1016/j.nantod.2020.100949

International Journal of Nanomedicine

Dovepress

Publish your work in this journal

The International Journal of Nanomedicine is an international, peer-reviewed journal focusing on the application of nanotechnology in diagnostics, therapeutics, and drug delivery systems throughout the biomedical field. This journal is indexed on PubMed Central, MedLine, CAS, SciSearch®, Current Contents®/Clinical Medicine, Journal Citation Reports/Science Edition, EMBase, Scopus and the Elsevier Bibliographic databases. The manuscript management system is completely online and includes a very quick and fair peer-review system, which is all easy to use. Visit <http://www.dovepress.com/testimonials.php> to read real quotes from published authors.

Submit your manuscript here: <https://www.dovepress.com/international-journal-of-nanomedicine-journal>